Available online at www.sciencedirect.com

ScienceDirect

Procedia CIRP 111 (2022) 144–147

www.elsevier.com/locate/procedia

12th CIRP Conference on Photonic Technologies [LANE 2022], 4-8 September 2022, Fürth, Germany

Discoloration of AISI 420 stainless steel in dependence of inter layer time during Laser-based Powder Bed Fusion

Jan Philipp Wahl[a,*], Robert Bernhard[a], Jörg Hermsdorf[a], Stefan Kaierle[a,b]

[a]*Laser Zentrum Hannover e. V., Hollerithallee 8, 30419 Hannover, Germany*
[b]*Leibniz Universität Hannover, Institut für Transport- und Automatisierungstechnik (ITA), An der Universität 2, 30823 Garbsen*

* Corresponding author. Tel.: +49-511-2788-346; fax: +49-511-2788-100. *E-mail address:* j.wahl@lzh.de

Abstract

Parts built by laser-based powder bed fusion (PBF-LB) experience intervals of heating and cooling during the powder deposition and the selective melting of successive layers. Short time intervals of cooling can lead to heat accumulation resulting in discoloration of AISI 420 (X20Cr13) stainless steel parts. Discoloration occurs due to the formation of oxide layers, which negatively affect the corrosion resistance. This process is determined by the time-dependent influence of temperature and oxygen.
Therefore, this study investigates effects of varied inter layer time on mechanical PBF-LB part properties and surface characteristics to prevent discoloration. EDX is used to analyze the chemical composition with regard to the chromium content as an indicator of reduced corrosion resistance. The results emphasize the need for implementing an minimum inter layer time greater than 12 s to prevent discoloration during the PBF-LB process with a layer thickness of 20 µm and a volume energy density of 113.3 J/mm³.

Keywords: Additive Manufacturing; Laser-Based Powder Bed Fusion; AISI 420; Inter Layer Time; Discoloration

1. Introduction

Laser-based powder bed fusion (PBF-LB) enables the production of final or near net shape parts and tools by building up geometries layer-by-layer. Stainless steel AISI 420 (X20Cr13) combines corrosion resistance with high mechanical strength and hardness. It is particularly suitable for tooling applications. Previous studies show mechanical properties of additively manufactured AISI 420 parts reaching ultimate tensile strength of 1670 MPa and hardness of 650 HV [1]. For the specified chromium steel this is based on the observation that high cooling rates in PBF-LB induce the formation of fine martensitic needles [1–3].

However, the layer wise build process also results in anisotropic mechanical properties and poses the challenge to dissipate heat from the part surrounded by a powder bed. Parts built by PBF-LB experience repeated intervals of heating and cooling. These occur during the selective melting and during the powder deposition of successive layers. The length of time intervals strongly depends on the areas to be exposed to laser light. Further parameters are scan speed, scan pattern, hatch distance and contour scans aside from the recoating process. Consequently, the part geometry contributes to its thermal history. It thereby influences the microstructure and the occurrence of defects.

To prove this, preliminary studies have investigated effects of the inter layer time described above during powder bed fusion of commonly processed materials such as AISI 316L stainless steel and Ti-6Al-4V. Extending the inter layer time intervals when processing Ti-6Al-4V can result in higher ultimate strength and finer microstructure but lower ductility. This is due to higher temperature gradients and the tendency to lack of fusion pores [4]. For the processing of AISI 316L it was shown that short inter layer time results in heat accumulation also considering built height. Short time intervals were found to increase the sub-grain size [5,6] and the occurrence of keyhole

10.1016/j.procir.2022.08.138

porosity while reducing the hardness [6]. In addition, a correlation between short time per layer and the discoloration of manufactured parts is noticeable [4,6,7]. It was demonstrated that introducing a high volume energy density enhances this effect [6].

Tempering colors in general are known to occur under the time-dependent influence of temperature and oxygen during fusion welding processes [8]. Different colors result from the interference on oxide layers. [9]. Table 1 shows an excerpt of a color scale for tempering colors of stainless steels and their layer thickness depending on the maximum temperature reached. Chromium and oxygen form a thin invisible passivating layer in air that inhibits the oxidation of the subjacent steel. A dense chromium oxide layer ensures corrosion resistance. It renews itself on the surface of stainless steels typically containing > 12 wt % alloyed chromium after it has been mechanically damaged when exposed to air [10]. Temperatures exceeding 400 °C change the formation of oxide layers that trend from a darker yellow towards a brown-red tempering color. This effect is linked to an increase of the oxide layer thickness up to 300 nm. The corrosion resistance decreases significantly especially against pitting since oxygen further diffuses into the material [8,9].

Table 1. Characteristics of stainless steel tempering colors according to [8,9]

Color	Temperature	Thickness
- (passivation layer)		≤ 5 nm
chrome yellow	< 400 °C	≤ 25 nm
golden yellow	500 °C	50-75 nm
brown-red	650 °C	75-100 nm
cobalt blue	> 800 °C	100-125 nm
light blue	1000 °C	125-175 nm
brown-grey	1200 °C	> 275 nm

Therefore, discoloration should be prevented with the help of inert gas during the process. Otherwise, they have to be removed by mechanical, chemical or electrochemical post-processing [8]. In contrast to conventional welding processes, the material is not only fused on parts' outer surfaces during PBF-LB. Instead, each layer temporarily represents the outermost surface that is exposed to the atmosphere with residual oxygen under the influence of temperature. In the case of heat accumulation during PBF-LB, the formation of undesirable oxide layers within the entire part is assumed.

The aim of this study is to investigate the correlation between inter layer time and the discoloration specifically for AISI 420 stainless steel parts. The specimens produced by PBF-LB are evaluated regarding the occurrence of oxide layers' tempering colors and their effect on the chemical composition of the outer surface and within the part. The investigation of the hardness depending on the inter layer time during AM reveals novel findings.

2. Material and Methods

2.1. Material

AISI 420 (X20Cr13) is a stainless chromium steel. The nitrogen gas atomized powder AM420S provided by Höganäs AB with a chromium content of 12.5 % (see Table 2) was used for powder bed fusion.

Table 2. Chemical composition of AISI 420 powder [11]

Element	Cr	Mn	Si	C	O	N	Fe
Content (wt %)	12.5	1.2	0.5	0.23	0.06	0.07	balance

The supplied nominal particle range is specified as 20-63 µm [11] for predominantly spherical particles as shown in Fig. 1 (a). High cooling rates during PBF-LB and the increased content of 0.23 % carbon favor the formation of a hard martensitic microstructure (see Fig. 1 (b)).

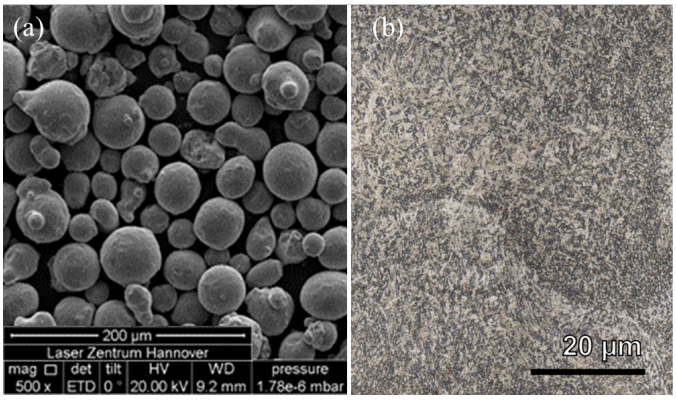

Fig. 1. (a) SEM image of AISI 420 powder (magnification 500x); (b) Light microscope image after etching with Adler's reagent (magnification 150x)

2.2. Machine Set up

The PBF-LB process was carried out on a TruPrint 1000 (TRUMPF GmbH & Co. KG, Germany). The machine includes a continuous wave ytterbium fibre laser, a galvanometric scanner and a f-theta lens. The system is characterized by a maximum laser power of 170 W at a wavelength of 1070 nm and a focus diameter of 30 µm. The circular build platform has a diameter of 100 mm. The maximum build height is 80 mm. The build platform was not heated and the oxygen content inside the process chamber was reduced to 200 ppm by filling it with the inert gas argon.

2.3. Experimental Method

The geometry dependent inter layer time can only be changed simultaneously for all test specimens of a layer. It therefor represents the only factor to be investigated in a one-factor experimental design with six factor levels.

Test specimens were designed by stacking cubes with an edge length of 5 mm vertically on top of each other and geometrically marking the levels' edges in the CAD model.

A previously developed combination of process parameters for part densities >99.9% was used to build the test specimens. The parameters for a layer thickness of 20 µm involve a laser

power of 145 W, a scanning speed of 640 mm/s and a hatch distance of 100 µm resulting in a volume energy density of 113.3 J/mm³. Moreover, a rotating chess pattern with 4 mm fields and contour scans were applied. Using the Materialise Magics software for pre-processing, block type support structures with a height of 3 mm were added to the specimens. Another 3 mm of solid material on top of the supports served as a solid base for building the first level.

The experimental run included a total of 20 test specimens positioned next to each other on the build platform. The number of cubes was gradually reduced by three per level. This reduces the ratio of the exposed area to the area of the build platform (see Table 3). Thereby, the interval of exposure and consequently the inter layer time was controlled.

Table 3. Factor levels of the experimental run

Level	No. of cubes	rel. Area melted (%)
1	20	6.37
2	17	5.41
3	14	4.46
4	11	3.50
5	8	2.55
6	5	1.59

2.4. Methods for analysis

Layers during PBF-LB were recorded using a 60 fps camera in order to examine the time intervals of the different levels by counting the frames. A Nexus 4000 (INNOVATEST Europe BV, Netherlands) was used to determine the hardness on the polished cross-section of a specimen with six levels. For each level, five crosswise-arranged indentations with a distance of 1 mm were measured. The HV 0.2 Vickers hardness was calculated according to DIN EN ISO 6507-1. The chemical composition of the as-built outer surface and the polished cross section of the inside of part was examined by means of energy dispersive x-ray spectography (EDX).

3. Results and Discussion

The following time intervals for one layer were determined during the PBF-LB process:

Table 4. Time intervals during the PBF-LB process

Interval	Mean time (s)	SD (s)
scanning of 1 specimen (25 mm²)	0.59	0.04
pause between scanning of specimens	0.05	0.02
pause between scanning specimens and coating	0.31	0.05
coating (100 mm/s, return run 250 mm/s)	2.83	0.05

The standard deviation (SD) of the scanning intervals results from varying scan vectors depending on the rotating chess pattern. Pauses vary due to different travel distances between specimens. Based on the examined time intervals, the inter layer time was calculated taking into account the number of cubes for levels 1-6 (see Table 5). The calculated time values show a reduction of the inter layer time of approximately 1.9 s as a consequence of removing three cubes per level.

Table 5. Inter layer time and tempering colors of the experimental run

Level	Inter layer time (s)	Color	HV 0,2
1	15.72	-	498±22
2	13.83	-	496±29
3	11.93	-	523±9
4	10.04	chromium yellow	619±18
5	8.14	golden yellow	632±12
6	6.25	cobalt blue	619±13

Specimens of levels 1-3 in Fig. 2 showed no discoloration. In contrast, tempering colors were observed on the specimens' top surfaces of level 4-6. Starting from a light chrome yellow color of level 4, the discoloration develops into a darker golden yellow layer on top of level 5. On the top surfaces of level 6, color gradients were found. The discoloration included a dark yellow middle surrounded by brown-red areas and violet as well as cobalt blue colors towards the edges of the specimens. The applied chess pattern becomes apparent in the form of different color gradients. The side view of the specimen in Fig. 2 (b) demonstrates that discoloration begins just above the edge between level 3 and 4. In addition, the discoloration visible on their side surfaces is not the same for the entire level. In fact, the discoloration changes with the built height. It can thus be concluded that the temperature continued to rise even within the levels 4-6 built at constant inter layer time. This leads to the interpretation that a limit for the inter layer time was exceeded, above which the energy input via laser radiation for each layer was higher than the heat that was dissipated during the intervals of cooling. Consequently heat accumulation occurred. According to Table 1 the discoloration indicates that temperatures of over 650 °C led to the formation of oxide layers on the edges of level 6 specimens.

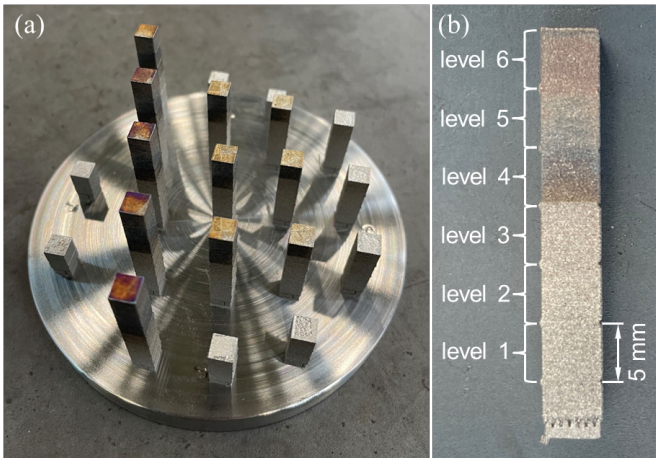

Fig. 2. (a) As-built specimens on the build platform and (b) side view of a specimen after removal

Furthermore, a significant increase in hardness was measured for levels 4-6 in comparison with levels 1-3. The reason for this could be carbide precipitation. During tempering of AISI 420 (X20Cr13) steel, chrome-rich carbides are formed in the temperature range of between 400°C and 600°C [12]. The associated chromium depletion reduces the resistance against intergranular corrosion [12]. Therefore, it is expected that an inter layer time of less than 12 s, led to a critical

reduction in corrosion resistance also for the yellowish discolored specimen of level 4 and 5.

Due to their low thickness, oxide layers could not be detected by EDX line scans. Instead, the chemical composition in an area of approx. 400 x 600 µm was qualitatively compared for the levels 1-6 using EDX (see Table 6 and Table 7).

In accordance with the discoloration of the specimen, the oxygen content of the as built sample was almost constant for levels 1-3. The oxygen content increased in the higher levels and reached a > 2.5 times higher value in level 6. However, limitations of EDX analysis for quantifying light elements such as oxygen have to be considered. Oxygen weight percentages of the cross section did not confirm this trend for the chemical composition inside the part and showed a much lower oxygen content overall.

Table 6. EDX analysis results of the as built outer surface

element	weight %					
	1	2	3	4	5	6
C	10.8	10	10.4	9.5	7.9	9.4
O	6.7	6.3	7.2	10.3	14	18.5
Si	1.3	1.3	1.3	1.3	1.3	1.6
Cr	11.5	11.8	11.6	11.3	11.5	10.6
Mn	2.2	2	1.9	2.1	2	2.6
Fe	67.6	68	67.6	65.5	63.4	57.3

Table 7. EDX analysis results of the polished cross section

element	weight %					
	1	2	3	4	5	6
C	8.7	9.6	10.1	10.6	10.4	10.9
O	1.4	1.4	1.6	1.3	1.1	1.4
Si	0.7	0.7	0.7	0.7	0.7	0.7
Cr	11.5	11.2	11.2	11.2	11.3	11.2
Mn	0.9	0.8	0.8	0.8	0.8	0.7
Fe	76.8	76.3	75.6	75.4	75.5	75.2

This indicates minor diffusion of oxygen in areas within the part. Due to the PBF-LB process principle, the outer surfaces remains in contact with residual oxygen in the powder bed for a longer time under the influence of heat from higher layers, while the inner area of the part is covered during the fusion of the subsequent layer. The increase in hardness measured on the polished cross section surface of level 4-6 is not accompanied by a change in the chemical composition. Therefore, subsequent investigation of the microstructure is required to determine carbide precipitates or other potential causes such as grain refinement or changes in the crystallographic texture.

4. Conclusion

This study shows that the inter layer time during laser-based powder bed fusion is a crucial factor for processing AISI 420 stainless steel. The smaller the area to be scanned with constant process parameters, the shorter the inter layer time. Experimental investigations proved that dropping below a time limit can lead to the discoloration of PBF-LB parts. Based on the occurring tempering colors, conclusions were drawn about the heat accumulation and resulting maximum temperatures above 650°C. It was hypothesized that short inter layer time intervals favor the formation of thick oxide layers on top of every layer. However, a consequential change in the chemical composition inside the part could not be proven by the methods used. EDX analysis of the outer part surface indicates an enhanced diffusion of oxygen at short inter layer times, though. In the case of processing AISI 420 stainless steel, an increase in hardness was observed in discolored areas. This effect is most likely associated with microstructural changes, for example with the precipitation of chromium-rich carbides. The microstructural analysis is subject of future research that should also examine the accompanying reduction of corrosion resistance.

To avoid negative effects of discoloration during PBF-LB with residual oxygen in the process chamber, implementing a minimum inter layer time tailored to the material and process parameters is critical. In order to transfer the results, further influencing factors such as machine specific ambient conditions as well as the built height and the geometry in lower sections of the parts including support structures must be investigated.

References

[1] Saeidi K, Zapata DL, Lofaj F, Kvetkova L, Olsen J, Shen Z, Akhtar F. Ultra-high strength martensitic 420 stainless steel with high ductility. Additive Manufacturing 2019;29:100803.
[2] Nath S. Process-property-microstructure relationships in laser-powder bed fusion of 420 stainless steel; 2018.
[3] Liverani E, Fortunato A. Additive Manufacturing of AISI 420 Stainless Steel: processes validation, defects analysis and mechanical characterization in different process and post-process conditions 2021.
[4] Torries B, Shao S, Shamsaei N, Thompson SM. Effect of Inter-Layer Time Interval on the Mechanical Behavior of Direct Laser Deposited Ti-6Al-4V; 2016.
[5] Yadollahi A, Shamsaei N, Thompson SM, Seely DW. Effects of process time interval and heat treatment on the mechanical and microstructural properties of direct laser deposited 316L stainless steel. Materials Science and Engineering: A 2015;644:171–83.
[6] Mohr G, Altenburg SJ, Hilgenberg K. Effects of inter layer time and build height on resulting properties of 316L stainless steel processed by laser powder bed fusion. Additive Manufacturing 2020;32:101080.
[7] Mohr G, Scheuschner N, Hilgenberg K. In situ heat accumulation by geometrical features obstructing heat flux and by reduced inter layer times in laser powder bed fusion of AISI 316L stainless steel. Procedia CIRP 2020;94:155–60.
[8] Ammann T. Formieren beim Schweißen; 2012.
[9] Schuler V, Twrdek J. Praxiswissen Schweißtechnik. Wiesbaden: Springer Fachmedien Wiesbaden; 2019. p. 526-535
[10] Schumann H, Oettel H, editors. Metallografie. Weinheim: Wiley; 2004. p. 710-714
[11] Höganäs AB. Datasheet AM 420S; 2020.
[12] Berger C, Kloos K. Eigenschaften und Verwendung der Werkstoffe. In: Grote KH, Feldhusen J., editors. Dubbel: Taschenbuch für den Maschinenbau. 21st ed. Berlin, Heidelberg: Springer-Verlag; 2005. pp. E47-E50